Behavior of Si Photoelectrodes under High Level Injection Conditions. 1. Steady-State Current−Voltage Properties and Quasi-Fermi Level Positions under Illumination

Ming X. Tan, C. N. Kenyon, Olaf Krüger, and Nathan S. Lewis*

Division of Chemistry and Chemical Engineering, California Institute of Technology, Pasadena, California 91125

Received: August 14, 1996; In Final Form: December 3, 1996[⊗]

The behavior of the quasi-Fermi levels of electrons and holes at various semiconductor/liquid interfaces has been probed through the use of thin, high purity, low dopant density single crystal Si photoelectrodes. Since standard Air Mass 1.5 illumination is sufficient to produce high level injection conditions in such samples, minimal electric fields can be present near the solid/liquid interface. Under these conditions, efficient charge separation relies on establishment of kinetic asymmetries at the back contacts while effectively sustaining photogenerated carrier concentration gradients in the photoelectrode. These conditions were achieved for Si/CH_3OH interfaces in contact with the 1,1′-dimethylferrocene$^{+/0}$, cobaltocene$^{+/0}$, methyl viologen$^{2+/+}$, and decamethylferrocene$^{+/0}$ redox couples. For redox couples having energies near the top of the Si valence band, such as 1,1′-dimethylferrocene$^{+/0}$, the sample acted like an n-type photoelectrode, yielding large photovoltages for collection of electrons at the back contact and small photovoltages for collection of holes. For redox couples having energies near the bottom of the Si conduction band, such as cobaltocene$^{+/0}$, the sample acted like a p-type photoelectrode, yielding large photovoltages for collection of holes at the back contact and small photovoltages for collection of electrons. The Si sample exhibited both photoanodic and photocathodic currents in contact with redox couples having electrochemical potentials in the middle of the Si band gap. A simple explanation, based on the fundamental carrier statistics of semiconductor/liquid contacts under illumination relative to the situation at equilibrium, is advanced to describe this behavior. This explanation is also applicable to a description of the photovoltage behavior of semiconductor particles and to undoped photoconductive semiconductor electrodes that are operated under high level injection conditions. In additional experiments, measurement of the apparent electrochemical potentials of electrons and holes in contact with various redox couples has allowed quantification of the amount of recombination and experimental determination of the separation of the quasi-Fermi levels for various redox couples at the semiconductor/liquid contact. These measurements are important to verification of key elements of the Shockley−Read−Hall and Marcus−Gerischer theories for semiconductor/liquid junctions.

I. Introduction

A frequently cited advantage of semiconductor/liquid contacts for chemically based solar energy conversion is their efficient quantum yield for charge separation, resulting from the presence of a strong electric field at the semiconductor/liquid junction.[1−13] In molecular solar energy conversion systems, charge separation is achieved primarily through the use of chemical potential gradients.[14−26] In these systems, back-electron-transfer processes are usually significant unless substantial free energy is sacrificed in the charge separation steps.[27−34] In contrast, charge carriers created by light absorption near a semiconductor/liquid contact are rapidly separated by the interfacial electric field, producing a photocurrent arising primarily from charge separation due to drift.[1−13] These separated charge carriers then diffuse through the electrode and are collected to perform useful work.[1−13,35,36] Most efforts to optimize photoelectrochemical cells for solar energy storage have sought to increase the interfacial electric field strength, thus increasing the effect of drift on charge separation in the near-surface (depletion) region of the solid. The Gärtner model for photocurrent collection,[37] and the "dead-layer" model for determining the radiative luminescence yield of injected charge carriers, are analytical examples of photoelectrochemical behavior that embody this strategy.[38−41] Such an approach has been quite successful to date and has resulted in numerous stable photoelectrochemical cells having solar energy conversion efficiencies exceeding 10% under 1 Sun, Air Mass 1.5 illumination conditions.[42−45]

This approach has limitations, however, because there are practical constraints on the maximum electric field strength that can be achieved for a given solid/liquid contact while simultaneously preventing recombination in the bulk of the crystal.[46−48] The single crystal n-Si/CH_3OH−1,1′-dimethylferrocene $(Me_2Fc)^{+/0}$ contact is one well-documented system for which variation in dopant density, and the resulting variation in electric field strength at the solid/liquid contact, have been explored in detail.[45,49] In this system, increases in dopant density (N_d) produce increases in the open-circuit photovoltage (V_{oc}) until $N_d > 10^{17}$ cm^{-3}. At higher dopant densities, Auger recombination and other bulk recombination processes result in a net increase in recombination[50−52] and thus effect a reduction in V_{oc}.[45,49] An alternative approach to charge separation is therefore required if this photovoltage limit is to be exceeded.

Similar considerations apply to solar energy conversion devices that utilize colloidal semiconductors or slurries of semiconducting particles as the primary light absorbers.[53−59] In general, minimal electric fields exist within a single semiconducting particle because the dimensions of such solids are smaller than the possible depletion region width for the semiconductor/liquid interface of concern.[11,60,61] Consequently, charge separation in these systems must rely on kinetic differences for collection of photogenerated charge carriers at

* To whom correspondence should be addressed.
[⊗] Abstract published in *Advance ACS Abstracts,* February 1, 1997.

S1089-5647(96)02483-2 CCC: $14.00

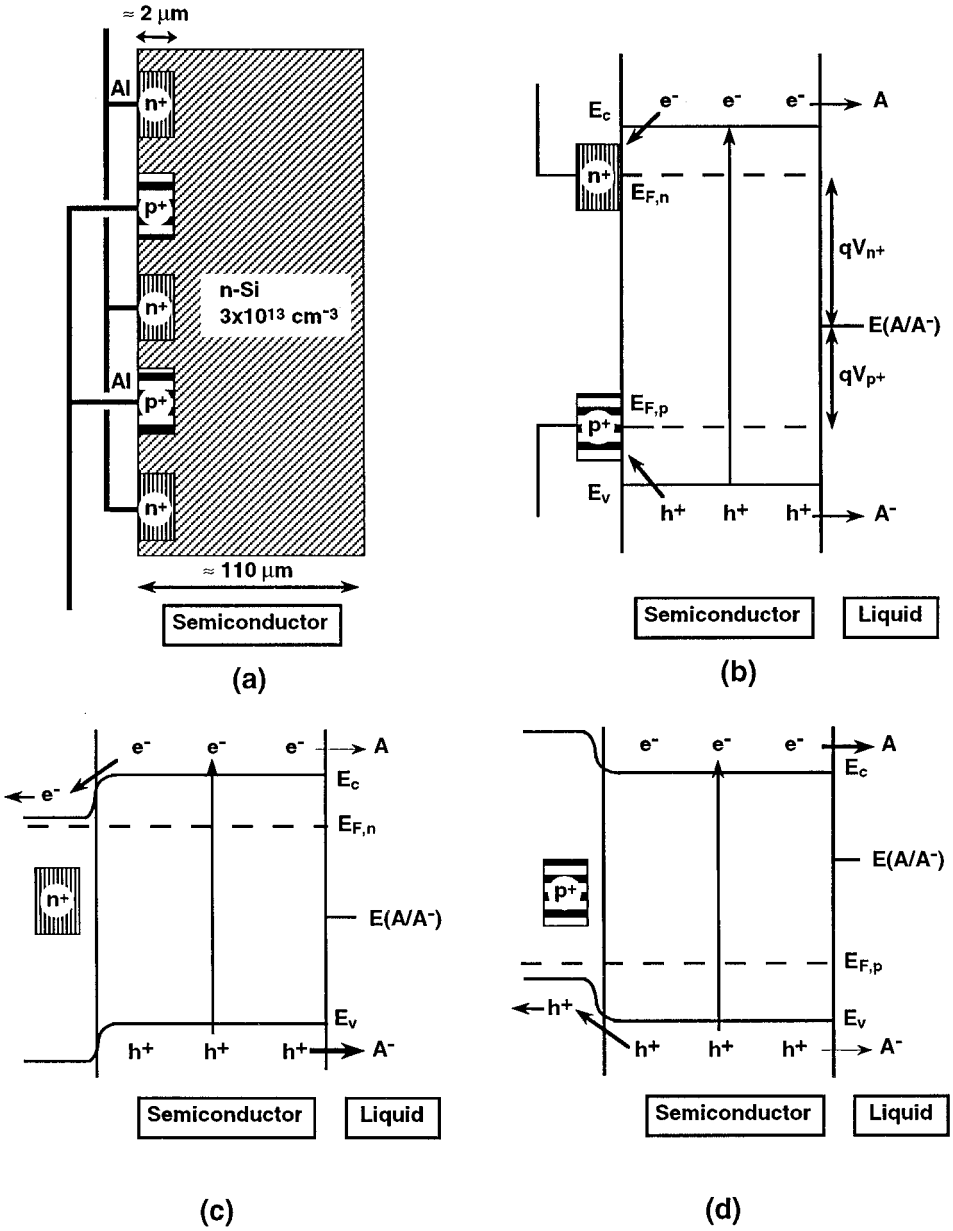

Figure 1. (a) Schematic representation of the high purity Si sample showing the n^+ and p^+ back contacts. (b) Band diagram of a Si/liquid junction under high level injection, open-circuit conditions. $\mathbf{E}_c$ and $\mathbf{E}_v$ represent the energies of the conduction band and valence band edges of the semiconductor, respectively. At the semiconductor/liquid interface, electrons and holes can recombine through reactions with the electron acceptor (A) and donor (A^-) species in the solution. V_{n+} and V_{p+} are the potentials measured at the n^+ and p^+ back points against the solution potential ($\mathbf{E}(A/A^-)/q$). The quasi-Fermi levels of electrons and holes are related to the measured potentials by $\mathbf{E}_{F,n} = qV_{n+}$ and $\mathbf{E}_{F,p} = qV_{p+}$. (c) Band diagram of the junction under potentiostatic control of the n^+ contact points. Electrons are collected from the back of the sample (n^+ region), and holes are collected in the solution. Because of the lack of a significant electric field at the interface to effect charge separation, electrons can also react with the solution. (d) Band diagram of the junction under potentiostatic control of the p^+ contact points.

various points of the particle, as is the case for most molecular photovoltaic systems. Such kinetic asymmetries are required in order to establish a nonuniform concentration profile that will induce carrier movement through diffusion. Because establishing controlled, significant rate constant asymmetries on the entire surface of a given particle is very difficult, most applications of particulate semiconductors that proceed with significant quantum yield are systems in which back-reactions are suppressed thermodynamically. This is feasible because the overall chemical transformations driven in such systems are exoergic. Well-studied examples of such processes include the TiO_2-catalyzed photooxidation of organics in water[6,62−72] and the CdS-catalyzed oxidation of H_2S.[11,60,73,74]

In the present work, we describe an alternative approach to obtaining efficient photoelectrochemical charge separation.[75,76] A thin, high purity, low dopant density sample of single crystal Si, with an extremely long minority carrier lifetime, is used as a photoelectrode (Figure 1). Steady-state, 1 Sun, Air Mass 1.5 illumination of this photoelectrode will produce high level injection conditions in which the concentration of photogenerated majority carriers exceeds the majority carrier concentration in the solid in the absence of illumination. Under such conditions, any electric fields, and therefore any drift currents, will be minimized at the solid/liquid contact. In order to obtain efficient charge separation in this system, concentration gradients driven by diffusion must be sustained throughout the crystal. This has been accomplished through the formation of ohmic-selective contacts, which only collect either electrons or holes, at the back side of the sample (Figure 1a,b). Due to this kinetic asymmetry, one carrier type will be collected at the back contact, while the other carrier will be forced to move by diffusion towards the solid/liquid contact (Figure 1c,d). Provided that

recombination in the bulk and at the surface of the crystal can be minimized, this approach should provide a method to separate charge with high quantum yield while circumventing the photovoltage limitations that are exhibited by devices operating under low level injection conditions.

Another advantage of this type of photoelectrode is that the ohmic-selective electrical contacts at the back of the sample provide a convenient monitor of the electrochemical properties of each individual carrier type, even while the sample is being illuminated. The measured potentials at each set of point contacts yield information on the apparent electrochemical potentials, or "quasi-Fermi levels", of the carriers in the solid.[35,77−79] Such measurements, described in this work, have allowed us to quantify the amount of recombination and to determine experimentally the separation of the quasi-Fermi levels, for various redox couples at the semiconductor/liquid contact. These measurements are important to the verification of key elements of the Shockley−Read−Hall and Marcus−Gerischer theories for semiconductor/liquid junctions.

We note that in prior work molecular photovoltaic devices such as liquid crystal porphyrins have displayed significant photovoltages arising from asymmetric charge carrier quenching processes.[80−82] Such systems have not, however, produced significant quantum yields for charge collection. A change in the direction of photocurrent with various contact configurations has been reported for thin film electrodes fabricated from nearly intrinsically doped amorphous hydrogenated Si, with the photocurrent behavior ascribed primarily to the sign and magnitude of the electric field across the sample under equilibrium conditions, as opposed to the kinetic approach to charge separation described herein.[83,84] Thin films of nanocrystalline semiconductors, such as CdSe, have shown photocurrents that change sign in response to changes in the materials structure and contacts, although the mechanism of these changes is not well-understood at present and the photovoltage was relatively low for the samples studied to date.[85] Dye-sensitized nanocrystalline TiO_2 films are thought to utilize carrier concentration gradients to produce photocurrents under illumination, but these systems are thought to be majority carrier devices in which only one carrier, the electron, can diffuse and be kinetically selected at the back contact.[59,86,87] The present studies are important to establish whether it is possible, in systems with low surface recombination rates and low bulk recombination rates, to use diffusionally driven concentration gradients to collect selectively one type of mobile charge carrier (rejecting the other mobile charge carrier) and simultaneously produce a high quantum yield, large photovoltage, and high energy conversion efficiency at the solid/liquid interface.

II. Experimental Section

The (100)-oriented Si samples were solid-state solar cells provided by SunPower Corp. The Si wafer thickness was initially 120 ± 5 μm, and the total area of each square sample was 1.44 cm^2. The float-zone Si substrate was slightly n-type with a dopant concentration of 3×10^{13} cm^{-3}. The minority carrier lifetime in these samples exceeded 1 ms.

Highly doped n^+ (sheet resistivity 8−10 Ω/□) and p^+ (sheet resistivity 20 Ω/□) contact points were fabricated onto the back of the sample using standard optical lithography methods. Aluminum contacts were then deposited on top of the implanted contact points. Each point contact was approximately 10×10 μm in area and was approximately 2 μm deep. The n^+ and p^+ points were spaced ≈20 μm apart, and silicon dioxide passivation layers were deposited between the points. This layout minimized the leakage current between the n^+ and the p^+ points. The front of the Si was anisotropically etched and then coated with a SiO_2 passivation layer, followed by coating with a layer of titanium dioxide. The SiO_2 layer minimized the surface recombination of electrons and holes in contact with air ambients, while the anisotropic etching profile and the TiO_2 coating were used to minimize optical reflection losses.

After receipt of the sample, separate electrical wires were soldered onto the Al patches that had been connected electrically to the diffused n^+ and p^+ points. The electrical leads were passed through glass tubing, and the back and edges of the cell were then sealed to the glass tubing using white epoxy resin (Dexter Corp.). This process protected the wires that contacted the n^+ and p^+ regions from exposure to the electrolyte solutions. As a result of this process, the front surfaces of photoelectrodes had typical exposed areas of 1.1 cm^2.

Before use, the electrodes were soaked in 48% HF(aq) for 6 min to remove the SiO_2 layer and to undercut the TiO_2 layer. The TiO_2 was then removed from the Si surface through use of a cotton swab. The exposed electrode material was etched in a solution of HNO_3:CH_3COOH:HF (v/v ratio 15:5:2) for 1 min, followed by a 10 s etch in 48% HF(aq). X-ray photoelectron spectroscopic (XPS) studies of this electrode surface confirmed that the TiO_2 layer had been completely removed by this etching procedure. The etching process reduced the sample thickness by 8 ± 1 μm (as measured with a micrometer).

Photoelectrochemical cells were prepared using dry methanol or tetrahydrofuran (THF) as the solvent. Redox couples and electrolytes were prepared according to procedures described previously.[49] Etchant solutions were prepared using reagent grade 69% HNO_3 (VWR), glacial CH_3COOH (Fischer), and transistor grade 48% HF(aq) (Mallinckrodt).

Photoelectrochemical experiments were performed in a single compartment air-tight Pyrex cell using an ELH-type tungsten−halogen bulb as the illumination source.[88] Pt wires and foils were used as the reference and auxiliary electrodes, respectively. All cell potentials were referenced to a saturated calomel electrode (SCE). Prior to each electrochemical experiment, the photoelectrode was etched in 48% HF(aq) for 20 s to remove any native oxides on the Si surface. The current density−voltage ($J-V$) characteristics of the high purity Si/liquid junction were then obtained with the n^+ or the p^+ contacts connected to the working electrode input of the potentiostat. $J-V$ data were recorded using an EG&G Princeton Applied Research Model 173 potentiostat/175 voltage programmer that was interfaced to a Houston Instruments Model 2000 chart recorder. The open-circuit potential at the contacts that were not under potential control was monitored against a separate Pt wire that was immersed in the electrolyte solution. These open-circuit voltage data were obtained using a Keithley Model 177 digital voltmeter.

External quantum yield measurements were performed at illumination intensities sufficient to achieve high level conditions in the Si sample. At 514.5 and 457.9 nm, excitation was provided by the single-line outputs of a Coherent Inc. Model 70-5 Ar^+ laser. A Coherent Inc. Model 890 continuous-wave Ti:sapphire laser, pumped by the all-lines output of the same Ar^+ laser, was employed for all other wavelengths. In both cases, the laser beam was expanded using a 40× magnification Gallilean telescope and was passed through a Pyrex slide to produce two beams, one acting as a sample beam and the other as a reference beam. The intensity of the sample beam was determined by measuring the current produced in a calibrated Si photodiode (United Detector Technology). Simultaneous measurements of the reference beam intensity were performed by monitoring the current produced in an uncalibrated Si

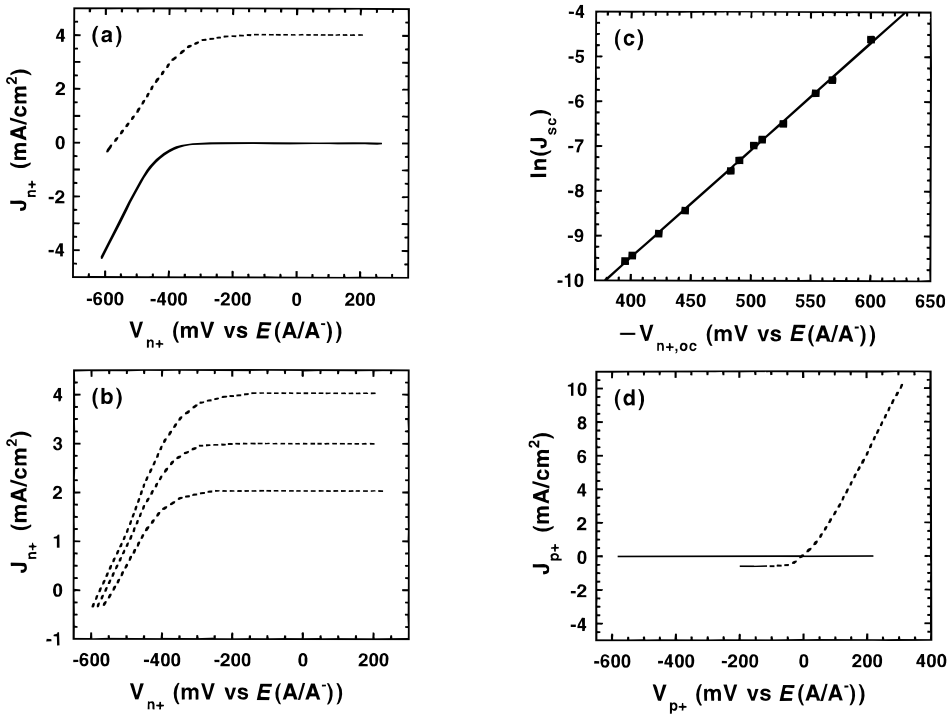

Figure 2. (a) Current density−voltage properties for the high purity, lithographically patterned n-Si samples in contact with $CH_3OH-LiClO_4-Me_2Fc^{+/0}$ when the potential was applied to, and current collected at, the n^+ point contacts. The dashed curve represents the $J-V$ properties under illumination (Si/CH_3OH−1.0 M $LiClO_4$−148 mM Me_2Fc−5.0 mM Me_2FcBF_4, E(A/A$^-$) = 115 mV vs SCE). The light intensity was adjusted to yield the desired photocurrent. The solid line represents the dark $J-V$ properties (Si/CH_3OH−1.0 M $LiClO_4$−31 mM Me_2Fc−32 mM Me_2FcBF_4, E(A/A$^-$) = 203 mV vs SCE). (b) Current density−voltage properties for n-Si/CH_3OH-$Me_2Fc^{+/0}$ contacts at several light intensities (Si/CH_3OH−1.0 M $LiClO_4$−148 mM Me_2Fc−5.0 mM Me_2FcBF_4, E(A/A$^-$) = 115 mV vs SCE). In all three instances the current in reverse bias represents the light-limited anodic photocurrent. (c) Natural logarithm of the short-circuit photocurrent density (in A cm^{-2}) collected at the n^+ points vs the open-circuit voltage measured at the same contacts for Si/CH_3OH−1.0 M $LiClO_4$−148 mM Me_2Fc−5.0 mM Me_2FcBF_4 (E(A/A$^-$) = 115 mV vs SCE). The slope of the line yields a diode quality factor of 1.6. (d) Current density−voltage properties for Si samples in contact with $CH_3OH-LiClO_4-Me_2Fc^{+/0}$ when the potential was applied to, and current collected at, the p^+ point contacts. In the absence of illumination (solid line; Si/CH_3OH−1.0 M $LiClO_4$−31 mM Me_2Fc−32 mM Me_2FcBF_4, E(A/A$^-$) = 203 mV vs SCE) the sample exhibited a large resistance to current flow in either direction. Under high level illumination, however, essentially ohmic behavior was observed (dashed line; Si/CH_3OH−1.0 M $LiClO_4$−148 mM Me_2Fc−5.0 mM Me_2FcBF_4 E(A/A$^-$) = 115 mV vs SCE). The plateau of the current observed at negative bias under illumination was due to mass-transfer limitations.

photodiode. After calibration had been performed, light-limited currents were determined for the electrode sample of interest (maintained under potentiostatic control) while the intensity of the reference beam signal was measured concurrently. The external quantum yield of the photoelectrode at a given wavelength was then calculated by dividing the signal obtained from the electrode by that obtained from the calibrated diode, multiplying the result by the absolute quantum yield of the calibrated photodiode (as specified by the manufacturer), and correcting for any beam intensity differences recorded on the uncalibrated diode used to monitor fluctuations in the laser beam intensity during the experiments.

III. Results

Two methods were used to demonstrate that the Si photoelectrodes investigated herein were operating under high level injection conditions. The first method depended on an analytical comparison of the open-circuit voltage, V_{oc}, observed experimentally to the upper limit for V_{oc} expected theoretically under low level injection conditions, as specified by the Shockley diode equation. The second method utilized a change in the direction of photocurrent in response to imposed diffusion gradients at the back side of the sample.

A. Si/$CH_3OH-Me_2Fc^{+/0}$ Contacts. *1. Comparison of the Photovoltage to the Theoretical Upper Limit for Low Level Injection Conditions.* Figure 2a displays the $J-V$ behavior of Si/$CH_3OH-Me_2Fc^{+/0}$ contacts when the n^+ points were biased potentiostatically relative to the solution potential, E(A/A$^-$). The $J-V$ behavior is typical of an n-type Si/CH_3OH-$Me_2Fc^{+/0}$ contact. Collection of electrons at the back of the sample produced $J-V$ behavior like that expected for an n-type photoelectrode, with anodic photocurrent and rectification to anodic current flow in the dark. Figure 2b depicts the $J-V$ properties of this junction for three different light intensities. Lower short-circuit photocurrent density values, J_{sc}, produced lower open-circuit photovoltages between the n^+ points and E(A/A$^-$), denoted herein as $V_{n+,oc}$, with a plot of ln(J_{sc}) vs $V_{n+,oc}$ (Figure 2c) having a slope of -24 V^{-1}, i.e., a diode quality factor of 1.6. A $V_{n+,oc}$ value of -550 mV was measured under illumination sufficient to provide a J_{sc} of 3.5 mA cm^{-2}.

Calculation of the upper limit on V_{oc} for minority carrier diffusion/recombination processes under low level injection, as described by the Shockley diode equation, yields a maximum $|V_{n+,oc}|$ value of 380 mV under these experimental conditions. This value was obtained using eq 1[46,48,89]

$$V_{oc} = \frac{kT}{q} \ln\left(\frac{J_{ph} L_p N_d}{q D_p n_i^2}\right) \quad (1)$$

where k is the Boltzmann constant, T is the temperature (297 K), q is the elementary charge, J_{ph} is the light-limited photocurrent density (3.5 mA cm^{-2}), L_p is the diffusion length (which was assumed to be equal to the sample thickness, 1×10^2 μm, for this high purity sample), D_p is the diffusion coefficient of

TABLE 1: External Quantum Yield Measurements for n-Si/$CH_3OH-Me_2Fc^{+/0}$ Contacts[a]

light intensity	λ, nm							
	1020	980	920	880	820	760	514.5	457.9
low[b]	0.49	0.56	0.71	0.67	0.72	0.80	0.42	0.23
high[c]			0.83	0.75	0.93	0.74		

[a] The solution potential was 130 mV vs SCE. [b] The quantum yield was measured at short-circuit current density levels between 1 and 10 mA cm^{-2}. [c] The quantum yield was measured at light intensities sufficient to provide short-circuit current densities greater than 10 mA cm^{-2} (typically around 12 mA cm^{-2}). Quantum yields are estimated to be accurate within ±0.07.

minority carriers (12 cm^2 s^{-1}), n_i is the intrinsic carrier concentration (1.45×10^{10} cm^{-3}) of the semiconductor, and N_d is the dopant density (3×10^{13} cm^{-3}). The observation of $|V_{n+,oc}|$ values significantly in excess of this theoretical upper limit confirmed that the specimens were being operated under high level injection conditions. These results indicate that the sample was "photodoped", so that the value of N_d produced by illumination of the semiconductor/liquid contact was significantly larger than N_d measured in the dark.

2. Response of J−V Behavior to Changes in the Back Contact Conditions. The *J*−*V* curves obtained when the p^+ points were biased relative to the solution potential exhibited significantly different behavior than those observed when the n^+ points were biased (Figure 2d). In the dark, the *J*−*V* behavior was consistent with that expected for a p^+ contact to a highly rectifying n-type Si/$CH_3OH-Me_2Fc^{+/0}$ contact, with substantial overpotentials for current flow in either bias direction of the p^+ points. However, under illumination, no rectification was observed, and the *J*−*V* behavior was essentially identical to that observed for deliberately doped p-type Si samples in contact with the $CH_3OH-Me_2Fc^{+/0}$ electrolyte. The dc differential resistance value under illumination (d*V*/d*I*), evaluated near zero faradaic current density, was a factor of ~10^4 lower than the dc differential resistance value observed for this contact in the dark. This provided further evidence that the samples were indeed in high level injection under the illumination conditions of this experiment.

3. Spectral Response Properties of Si/$CH_3OH-Me_2Fc^{+/0}$ Contacts in High Level Injection. The spectral response of Si/$CH_3OH-Me_2Fc^{+/0}$ contacts under high level injection conditions was obtained through use of monochromatic laser illumination. Measurements were performed at several photon energies, **E**, for which $\mathbf{E} > \mathbf{E}_g$, where $\mathbf{E}_g$ is the band gap energy of the Si sample. Table 1 presents the external quantum yield data as a function of wavelength for a representative Si/CH_3OH−1.0 M $LiClO_4$−58 mM Me_2Fc−2.0 mM Me_2FcBF_4 contact. The decline in external quantum yield at short wavelengths was primarily due to solution absorption, not to recombination at the solid/liquid contact. In addition, the lower quantum yields at 980 and 1020 nm were attributable to the smaller absorption coefficients of Si at these wavelengths.[46,90−95] This behavior was similar to that observed for n-Si/$CH_3OH-Me_2Fc^{+/0}$ contacts operated in low level injection, for which internal quantum efficiencies approach unity.[96] These data indicate that high quantum yields for charge separation were maintained under high level injection conditions regardless of whether the carriers were photogenerated within 1 μm of the solid/liquid contact or were generated virtually uniformly throughout the sample.

B. *J*−*V* Behavior of Si/THF−$CH_3OH-Me_{10}Fc^{+/0}$ and Si/$CH_3OH-MV^{2+/+}$ Contacts. Parts a and b of Figure 3 depict the *J*−*V* data obtained as a result of controlling the potential at the n^+ and p^+ points, respectively, of these Si samples in contact with THF−CH_3OH−decamethylferrocene $(Me_{10}Fc)^{+/0}$. Analogous data were also obtained for the Si photoelectrodes in contact with CH_3OH−methyl viologen $(MV)^{2+/+}$.[76,97] These two redox reagents have formal electrochemical potentials which are more negative than that of $Me_2Fc^{+/0}$. Thus, these redox couples were expected to produce smaller photovoltages between the n^+ points and the solution potential. In fact, prior to the experiments, it was not clear whether, in the presence of significant concentrations of both forms of the redox couple, substantial charge carrier separation could be obtained at such contacts because of the possibility of effective recombination due to faradaic capture of both electrons and holes at the solid/liquid junction.

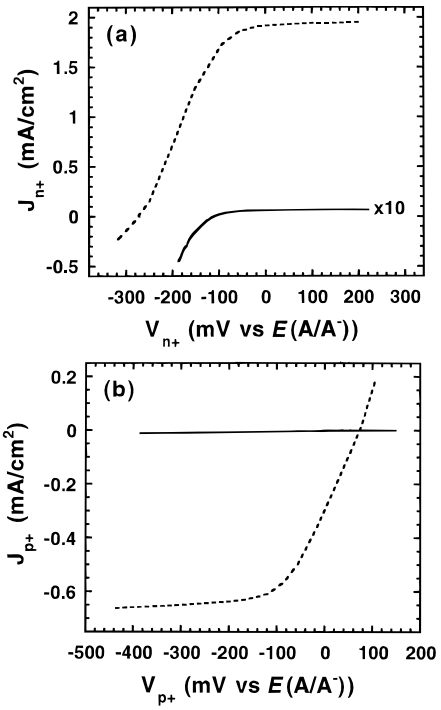

Figure 3. (a) Current density−voltage properties under illumination (dashed line), and in the dark (solid line), for a Si electrode in contact with 75% THF−25% CH_3OH (v/v)−1.0 M $LiClO_4$−14 mM $Me_{10}Fc$−17 mM $Me_{10}FcBF_4$ (E(A/A$^-$) = −22 mV vs SCE) when the potential was applied to, and current collected at, the n^+ point contacts. The ×10 indicates an amplification of the data collected in the dark for better comparison with the photocurrent density behavior. (b) Current density−voltage properties for a Si sample in contact with the same solution when potential was applied to, and current collected at, the p^+ point contacts. The *J*−*V* properties observed under illumination (dashed line) are like those typically seen for deliberately doped p-type Si photoelectrodes in contact with $Me_{10}Fc^{+/0}$. However, as was the case for these samples in contact with $Me_2Fc^{+/0}$, the dark *J*−*V* characteristics are substantially different, with large resistances to current flow in either direction being observed.

As displayed in Figure 3a, an anodic photocurrent and rectification to anodic current in the dark were observed when the electrical lead was connected to the n^+ points and these points biased to potentials positive of $V_{n+,oc}$. In contrast, as displayed in Figure 3b, when the lead to the n^+ points was disconnected and potential control was established at the p^+ points, the photocurrent changed sign, and the sample produced cathodic photocurrents and rectification to cathodic current in the dark under a negative bias relative to the open-circuit voltage measured between the p^+ points and the solution potential, $V_{p+,oc}$. The sample thus behaved like a photoanode or photocathode in contact with the same electrolyte solution, with the electrochemical properties of the solid/liquid contact entirely dictated by the contact arrangements at the back of the sample.

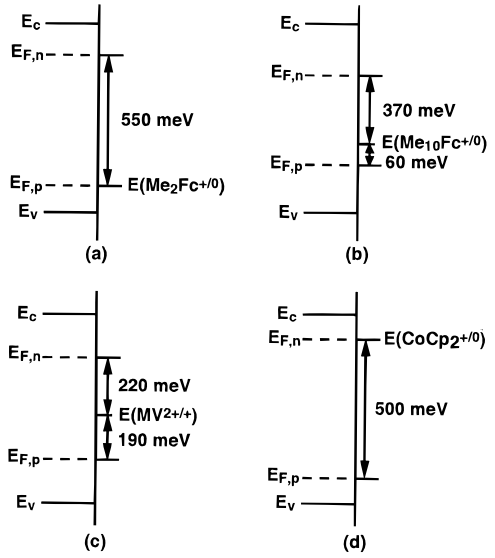

Figure 4. Positions of quasi-Fermi levels of electrons and holes at open circuit in various solutions, under illumination intensities sufficient to provide 3.5 mA cm^{-2} of photocurrent density.

Such behavior would not have been expected for samples operated under low level injection conditions, where the magnitude of the electric field at the solid/liquid contact would determine the rectification properties of the solid/liquid junction regardless of the electrical nature of the back contacts. This behavior provides further evidence that diffusion-driven concentration gradients determine the $J-V$ properties of these samples under the experimental measurement conditions.

The open-circuit photovoltages at the n^+ points for illuminated Si/THF−CH_3OH−$Me_{10}Fc^{+/0}$ and Si/CH_3OH−$MV^{2+/+}$ contacts were smaller in magnitude than those of Si/CH_3OH−$Me_2Fc^{+/0}$ contacts, while $V_{p+,oc}$ values increased monotonically as **E**(A/A^-) became more negative (Figure 4). Under a given illumination intensity, the sum of $|V_{n+,oc}|$ and $V_{p+,oc}$ was smaller for Si/THF−CH_3OH−$Me_{10}Fc^{+/0}$ and Si/CH_3OH−$MV^{2+/+}$ contacts than for Si/CH_3OH-$Me_2Fc^{+/0}$ contacts, indicating that recombination was greater for these systems than for the Si/CH_3OH−$Me_2Fc^{+/0}$ interface. As discussed below, this behavior is expected for contacting phases having energy levels in the middle of the Si band gap, with maximum $|V_{oc}|$ values being expected for redox potentials lying closer to either the conduction or valence band edge energies.

C. $J-V$ Behavior of Si/CH_3OH−$CoCp_2^{+/0}$ Contacts. The $J-V$ properties of Si/CH_3OH−cobaltocenium/cobaltocene ($CoCp_2^{+/0}$) contacts were also of interest. The CH_3OH−$CoCp_2^{+/0}$ redox system has a very negative electrochemical potential and, in the absence of band edge movement, would require efficient collection of electrons and efficient rejection of holes at the Si/liquid junction to develop a significant V_{oc}. Additionally, the low surface recombination velocity exhibited by Si/CH_3OH−$Me_2Fc^{+/0}$ contacts[13,98] is required in order to suppress recombination at the solid/liquid interface; otherwise, small V_{oc} values would be observed.

Figure 5 displays the $J-V$ behavior for Si/CH_3OH−$CoCp_2^{+/0}$ contacts at a variety of light intensities. Collection of electrons at the n^+ points led to nonrectifying, "ohmic" behavior in either the light or the dark. In contrast to the behavior for the Si/CH_3OH−$Me_2Fc^{+/0}$ contacts, the sample behaved exclusively as a photocathode, with collection of holes at the p^+ points leading to large $V_{p+,oc}$ values and significant cathodic photocurrents. At a constant photocurrent density, $V_{p+,oc}$ for Si/CH_3OH−$CoCp_2^{+/0}$ was significantly larger than that of Si/CH_3OH−$MV^{2+/+}$ and Si/THF−CH_3OH−$Me_{10}Fc^{+/0}$ contacts and was

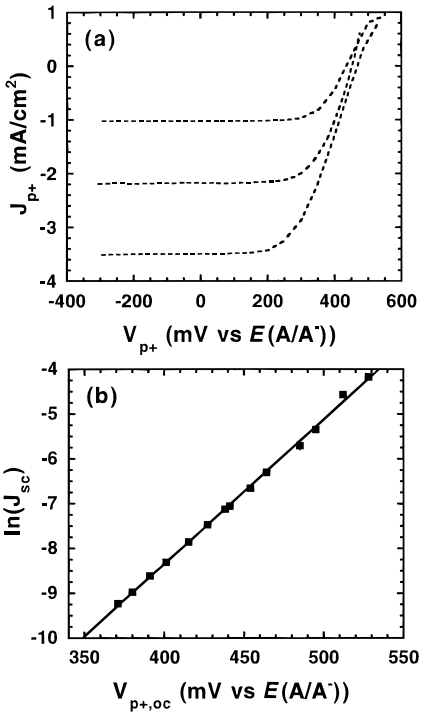

Figure 5. (a) Current density−voltage properties at several light intensities for a Si sample in contact with CH_3OH−0.90 M LiCl−2.3 ± 0.2 mM $CoCp_2$−45 mM $CoCp_2Cl$ (E(A/A^-) = −890 mV vs SCE) when the potential was applied to, and current collected at, the p^+ point contacts. (b) Natural logarithm of the short-circuit density vs the open-circuit voltage for Si/CH_3OH−0.90 M LiCl −2.3 ± 0.2 mM $CoCp_2$−45 mM $CoCp_2Cl$ (E(A/A^-) = −890 mV vs SCE). The slope of the line yields a diode quality factor of 1.2.

within 50 mV of $|V_{n+,oc}|$ for Si/CH_3OH−$Me_2Fc^{+/0}$ contacts (Figure 4). This illustrates that high V_{oc} values for these photoelectrodes are not unique to the $Me_2Fc^{+/0}$ system, which has an electrochemical potential located near the valence band edge energy, but can also be observed for the $CoCp_2^{+/0}$ system, which has an electrochemical potential located near the energy of the conduction band edge. Additionally, as for the $V_{n+,oc}$ values of the Si/CH_3OH−$Me_2Fc^{+/0}$ system, the $V_{p+,oc}$ values for the Si/CH_3OH−$CoCp_2^{+/0}$ system were higher than those calculated from the Shockley diode equation, again confirming the operation of these samples under high level injection conditions.

IV. Discussion

A. Current Density vs Voltage Properties of Si Samples under High Level Injection. The $J-V$ properties of these samples clearly demonstrate that it is possible to achieve efficient charge separation, and to produce significant photovoltages, using photoelectrochemical cells that do not have strong electric fields at their solid/liquid interface. Charge collection in the semiconductor can occur efficiently over such large distances because the carrier lifetime in this highly pure Si sample is sufficient that carriers created throughout the sample can reach the back contact region before recombining in the solid. In this regard, the samples can be viewed as extremely efficient photogalvanic "molecular photosensitizer" energy conversion devices. The efficiency improvements arise because of the long excited-state lifetimes, high charge carrier mobilities, and highly selective kinetic quenching characteristics that are obtainable using Si technology.

The behavior of Si/THF−CH_3OH−$Me_{10}Fc^{+/0}$ and Si/CH_3-OH−$MV^{2+/+}$ contacts was especially interesting in this regard. Since the back of the sample was separated by $>10^3$ Debye

lengths from the solid/liquid contact, the electric field strength at the solid/liquid interface under short-circuit conditions could not have been affected by the nature of the electrical connections made to the point contacts at the back of the specimen. Thus, efficient carrier separation and collection are possible merely by manipulating the boundary conditions at the back contact of the sample. The ability to completely reverse the direction of carrier movement, while maintaining a high quantum yield for charge separation and collection, provides strong evidence that diffusion-driven concentration gradients are primarily responsible for effecting charge separation at these solid/liquid contacts.

B. Dependence of the Photovoltages of Si Samples under High Level Injection on the Energetics of the Solid/Liquid Contact. The photovoltages obtained from such samples can be larger than those obtained from samples operated under more conventional, low level injection conditions. This improvement in photovoltage occurs because the high minority carrier lifetime of nearly intrinsically doped samples is maintained under illumination, while a significant concentration of carriers, required for negligible resistive losses in the sample, is produced from the photogenerated electron−hole pairs. The observation that these types of photoelectrodes can be induced to produce either anodic or cathodic photocurrents, with large photovoltages in either mode of operation, extends a specific strategy described previously (which used only n^+ contacts) to construct efficient photoelectrochemical cells operating under high level injection conditions.[99]

It is interesting to evaluate the principles governing the behavior of the photocurrent and photovoltage as a function of the redox couple and the contact geometry. Specifically, redox couples with very positive values of $\mathbf{E}(A/A^-)$ yielded large photovoltages for electron collection at the n^+ points and produced small photovoltages at the p^+ points, so that the illuminated electrode acted as if it were an n-type doped sample. In contrast, when the redox couple had a very negative electrochemical potential, the photoelectrode behaved as if it were a p-type doped electrode, producing large photovoltages at the p^+ points and small photovoltages at the n^+ points. A superficial analysis would imply that this behavior was fortuitous and that the $Me_2Fc^{+/0}$ redox couple, which has $\mathbf{E}(A/A^-)$ near the energy of the top of the valence band, $\mathbf{E}_v$, simply happened to have a relatively large capture rate constant for holes and a small capture rate constant for electrons, thereby producing a photoanodic current flow and also allowing the electron's effective electrochemical potential to deviate from equilibrium under illumination while not wasting energy in collection of the holes. A similar coincidence would then also be required for the $CoCp_2^{+/0}$ redox couple (having $\mathbf{E}(A/A^-)$ near the energy of the bottom of the conduction band, $\mathbf{E}_c$), except that this redox couple would need to collect electrons rapidly while fortuitously rejecting holes to produce a photocathodic current flow and a large photovoltage at the p^+ point contacts. Such preferential charge transfer of one carrier type or the other has been invoked previously to rationalize the photoelectrochemical behavior of nanocrystalline CdSe systems.[85] We demonstrate below that a more fundamental principle governs the photoelectrochemical behavior of the Si-based systems and, by extension, is likely applicable to other related systems that use intrinsically doped semiconductors under high level injection conditions.

1. Behavior of the Photocurrent. The directionality of the photocurrent observed in this work was not a function of the charge transfer kinetics at the solid/liquid contact, but instead was governed entirely by the boundary conditions imposed by the back contact. When the n^+ points were contacted, the photocurrents were always anodic in sign, regardless of the concentrations, ratio of oxidized to reduced species, or redox potentials of the redox couple in the solution. This situation held for redox couples having electrochemical potentials near the conduction band, in the middle of the band gap, or near the valence band of the semiconductor and therefore logically applies to contacts having a variety of electron/hole charge transfer rate constant ratios. Similarly, when the p^+ points were contacted, the photocurrents were cathodic in sign for all the types of solution contacts. This behavior is readily understood as electrons cannot pass through the back p^+-Si/intrinsic-Si junction. An ohmic back contact that collected both carrier types efficiently and simultaneously would simply lead to effective recombination and would produce small, if any, photocurrents or photovoltages for any type of redox couple. The data of Figures 2, 3, and 5, and the above discussion, fully support the conclusions that the direction of current flow is dictated by the back contact conditions and that preferential charge transfer rates of one carrier type or the other at the solid/liquid interface can affect the photovoltage, but not the photocurrent directionality, of an efficient photoelectrochemical cell under high level injection.

2. Behavior of the Photovoltage. Since the photovoltage is influenced by the nature of the solid/liquid contact (Figure 4), it is of interest to evaluate the factors controlling its behavior. The question involves the mechanism by which the sample appears to behave "n-type" when a system with a positive redox potential is present (Figure 2) and then appears to behave "p-type" when a system with a negative redox potential is present (Figure 5). A key point to explain this behavior is that the interfacial charge-transfer fluxes obey equations of the following form[13,100,101]

$$\text{hole flux} = k_p(p_s - p_{so}) \tag{2}$$

$$\text{electron flux} = k_n(n_s - n_{so}) \tag{3}$$

where k_p and k_n are the hole and electron capture rate constants, respectively, n_s and p_s are the electron and hole concentrations, respectively, at the semiconductor surface, and n_{so} and p_{so} are the equilibrium electron and hole concentrations, respectively, at the semiconductor surface. These expressions are reasonable because at equilibrium they yield no net interfacial hole flux or electron flux. Away from equilibrium, these equations indicate that the interfacial flux of electrons or holes is proportional to the charge carrier capture coefficient in effect at equilibrium multiplied by any deviation from the equilibrium charge carrier concentration in the nonequilibrium state. This latter relationship can be deduced by application of the principle of detailed balance to the semiconductor/liquid interface, with the simplifying assumption (used for the purposes of this discussion but not required for a general treatment) that the electrons and holes are thermalized to the lattice temperature under the nonequilibrium conditions of interest.

A second key point required to understand the observed behavior is that the electrochemical potential of electrons (i.e., the electron quasi-Fermi level), $\mathbf{E}_{F,n}(x)$, measured relative to the electrochemical potential of the solution ($\mathbf{E}_F = \mathbf{E}(A/A^-) = 0$ at equilibrium, by definition of the reference potential in this work) can be described at any position within the sample by[79,102]

$$\mathbf{E}_{F,n}(x) = -(kT)\ln(n(x)/n_o(x)) \tag{4}$$

Similarly, the quasi-Fermi level of holes, $\mathbf{E}_{F,p}(x)$, is given as

$$\mathbf{E}_{F,p}(x) = (kT)\ln(p(x)/p_o(x)) \tag{5}$$

The relations in eqs 2−5 are all that are needed in order to explain the photovoltage behavior observed experimentally for these photoelectrodes.

For the open-circuit condition to be met, no net current can flow across the solid/liquid interface. Thus, eqs 2 and 3 yield

$$k_p(p_s - p_{so}) = k_n(n_s - n_{so}) \quad (6)$$

Illumination creates excess electron and hole concentrations Δn and Δp, respectively, where $\Delta n \equiv n - n_o$ and $\Delta p \equiv p - p_o$ at any point in the solid. Using these definitions in a rearranged form of eq 6 yields the desired final relationships:

$$p_s/p_{so} = 1 + (k_n/k_p)(\Delta n_s/p_{so}) \quad (7)$$

$$n_s/n_{so} = 1 + (k_p/k_n)(\Delta p_s/n_{so}) \quad (8)$$

Equations 6−8 act as constraints (in addition to any other recombination mechanisms that operate in the sample) that will dictate the carrier concentrations and, thus, the quasi-Fermi levels $\mathbf{E}_{F,n}(0)$ and $\mathbf{E}_{F,p}(0)$ at the solid/liquid interface.

Although the hole and electron concentrations contain all of the fundamental information about the device, the experimental protocol used herein probes the voltages $V_{n+,oc}$ and $V_{p+,oc}$. It is therefore necessary to relate these quantities to the carrier concentrations. The potentials of the individual quasi-Fermi levels at the back of the sample, $E_{F,n}(d)$ and $E_{F,p}(d)$ (with $E_{F,n} = \mathbf{E}_{F,n}/q$ and $E_{F,p} = \mathbf{E}_{F,p}/q$), are equal to the voltages measured between the point contacts and the solution potential, which are determined experimentally as $V_{n+,oc}$ and $V_{p+,oc}$. Assuming the quasi-Fermi levels are flat throughout the sample (as validated by digital simulations; see accompanying papers) implies that $\mathbf{E}_F(d) = \mathbf{E}_F(0)$. This equality can be combined with eqs 4 and 5 to yield

$$V_{n+,oc} = -(kT/q)\ln(n_s/n_{so}) \quad (9)$$

$$V_{p+,oc} = (kT/q)\ln(p_s/p_{so}) \quad (10)$$

The implications of eqs 7−10 are first explored for a redox couple having $\mathbf{E}(A/A^-)$ near $\mathbf{E}_v$, such as $Me_2Fc^{+/0}$. For such a system, p_{so} is very large, and n_{so}, given by n_i^2/p_{so} where n_i is the intrinsic carrier concentration of the semiconductor, is correspondingly small. Consequently, it is expected that $\Delta n_s \leq p_{so}$, even under high level illumination. This implies that $p_s \approx p_{so}$, even for equal rate constants of electron and hole capture (eq 7). Under these conditions, eq 10 indicates that $V_{p+,oc} \approx 0$, and, thus, that the hole quasi-Fermi level will remain very close to the redox potential of the solution. However, since n_{so} is small, these same illumination conditions yield $n_s/n_{so} \gg 1$, and eq 9 then predicts a large value for $|V_{n+,oc}|$. In other words, this scenario produces $|V_{n+,oc}| \gg V_{p+,oc}$ and $V_{p+,oc} \approx 0$, in accord with the experimental observations for the Si/CH_3OH-$Me_2Fc^{+/0}$ junction (Figure 4).[103]

A similar argument can be developed for redox couples having $\mathbf{E}(A/A^-)$ near $\mathbf{E}_c$. In this case, the analysis described above would yield $n_s/n_{so} \approx 1$ and $p_s/p_{so} \gg 1$. This set of conditions would imply, according to eqs 9 and 10, that $V_{p+,oc} \gg |V_{n+,oc}|$ and $V_{n+,oc} \approx 0$. This is precisely the situation observed for the Si/CH_3OH-$CoCp_2^{+/0}$ contact (Figure 4). For $\mathbf{E}(A/A^-)$ in the middle of the semiconductor band gap, $n_s/n_{so} > 1$ and $p_s/p_{so} > 1$ at open circuit, and therefore both $V_{n+,oc}$ and $V_{p+,oc}$ will be substantial. This is exactly the behavior observed experimentally for $Si/THF-CH_3OH-Me_{10}Fc^{+/0}$ and $Si/CH_3OH-MV^{2+/+}$ contacts (Figure 4). It is therefore seen that the underlying semiconductor statistics that control the available free energy of an illuminated photoelectrode account for the experimental observations that the intrinsic Si sample appears to adjust its photoelectrochemical behavior to respond optimally to the redox potential of the solution, regardless of the actual values of the charge transfer rate constants of the system under study.

TABLE 2: Ratio of the Exchange Current Densities Calculated for Various Si/CH_3OH Contacts

	$V_{n+,oc}$ (mV)	$V_{p+,oc}$ (mV)	J_c^0/J_v^0
$Me_2Fc^{+/0}$	−550	<5	$<1.2 \times 10^{-10}$
$Me_{10}Fc^{+/0}$	−370	60	5.6×10^{-6}
$MV^{2+/+}$	−220	190	0.3
$CoCp_2^{+/0}$	<5	500	$>1.2 \times 10^{9}$

3. Behavior of the Partial Currents as a Function of the Energetics of the Semiconductor/Liquid Contact. The ability to probe experimentally the open-circuit voltages at the n^+ and p^+ points simultaneously provides an opportunity to compare quantitatively the exchange current densities (pseudo rate constants) for the conduction and valence band processes at a given semiconductor/liquid contact. The partial currents via the conduction (J_c) and valence bands (J_v) can be expressed as[78,79]

$$J_c = -J_c^0\left[\frac{n_s}{n_{so}} - 1\right] = -J_c^0\left[\exp\left(-\frac{qV_{n+}}{kT}\right) - 1\right] \quad (11)$$

$$J_v = J_v^0\left[\frac{p_s}{p_{so}} - 1\right] = J_v^0\left[\exp\left(\frac{qV_{p+}}{kT}\right) - 1\right] \quad (12)$$

where J_c^0 and J_v^0 denote the exchange current densities for electrons (via the conduction band) and for holes (via the valence band), respectively.

At V_{oc}, the net current is zero ($J = J_c + J_v = 0$). From eqs 11 and 12, this yields

$$\frac{J_c^0}{J_v^0} = \frac{\exp\left(\frac{qV_{p+,oc}}{kT}\right) - 1}{\exp\left(-\frac{qV_{n+,oc}}{kT}\right) - 1} \quad (13)$$

Thus, measurements of $V_{p+,oc}$ and $V_{n+,oc}$ provide the information necessary to compute the ratio J_c^0/J_v^0.

The computed values of J_c^0/J_v^0 for all the Si/CH_3OH contacts investigated in this work are summarized in Table 2. Redox couples having an electrochemical potential close to one of the energy bands show a significantly larger exchange current density for the transfer with that band than for the transfer to the other band. In other words, the ratio of J_c^0/J_v^0 increases if the redox potential is shifted more negative, i.e., closer to the conduction band. This behavior is also in accord with theoretical predictions[35,78] which had not yet, to our knowledge, been verified for outer-sphere redox systems at stable semiconductor/liquid contacts.[104]

4. Implications for Other Intrinsic Photoelectrodes. The treatment developed herein is also useful in explaining the behavior of intrinsically doped layers present in amorphous hydrogenated Si (Si:H) photoelectrodes. The photocurrent and photovoltage properties of such materials have been previously explained in terms of drift effects and the initial energetics of the solid/liquid and solid/back contacts.[83,84] In this explanation, the electric fields across such materials, produced by the energetic differences between the work functions of the liquid contact and the back contact, have been associated with the directionality of current flow and with the photovoltage properties of the system. In this approach, it is not apparent what the

direction of the photocurrent flow, or what the magnitude of the photovoltage, should be for any particular system. For example, when only the relative energetics of the back and front contacts are considered, it is not clear whether the electric field under illumination of an intrinsically doped semiconductor should develop with respect to the position of the valence or conduction band edge, and it is also unclear whether the sample should behave as a photoanode or photocathode when contacting a particular redox couple.

In contrast, the framework described herein accounts for the experimentally observed behavior of such systems. The intrinsic a-Si:H layer behaves as an n-type photoanode in an n^+-intrinsic/liquid configuration because of the back contact metallurgy, which kinetically prevents collection of holes and therefore induces only photoanodic currents. This occurs regardless of the front contact energetics. The p^+-intrinsic/liquid configuration of amorphous Si photoelectrodes produces the opposite photocurrent because of its p^+ back contact boundary conditions, not because of the energetics of the back contact work function relative to the redox potential of the liquid phase. Additionally, as discussed above, the fundamental statistics of the front contact system can be used to explain the experimental observations that significant photovoltages are obtained from the electron quasi-Fermi level for redox couples with positive redox potentials and from the hole quasi-Fermi level for redox couples with negative redox potentials. This formalism thus provides a unifying framework that can not only explain the observations to date on crystalline Si and amorphous hydrogenated Si but also allow the formulation of useful predictions for optimal energy conversion configurations from a variety of intrinsically doped devices operated under high level injection conditions.

V. Summary and Conclusions

The experiments described herein have shown that efficient charge separation and significant energy conversion efficiencies can be obtained for semiconductor/liquid contacts under high level injection conditions without relying primarily on drift to effect separation of the photogenerated charge carriers. Photocurrents in such samples can be either anodic or cathodic in sign, and this behavior is dictated exclusively by the kinetic charge carrier collection properties established by the metallurgy at the back (nonliquid) side of the semiconductor electrode. The interfacial charge carrier kinetics at the solid/liquid interface primarily affect the photovoltage and energy conversion efficiency of these junctions. The fundamental semiconductor statistics of junction equilibration have been shown to provide a simple explanation of the photovoltage properties of these samples and to explain which junctions will have the proper initial energetic differences to produce optimal energy conversion devices for a given contact configuration. These principles are of importance to understanding the photoelectrochemical behavior of bulk intrinsic semiconductor photoelectrodes, particulate semiconductor photoelectrode systems, and other photoelectrodes that are operated under high level injection conditions.

Acknowledgment. We acknowledge the National Science Foundation, Grant CHE-9634152, for support of this research. M.X.T. acknowledges the Link Foundation and W. R. Grace, Inc., for graduate fellowships, and O.K. acknowledges the Deutsche Forschungsgemeinschaft for a postdoctoral fellowship. We are grateful to Drs. R. Sinton and R. Swanson of Sunpower, Inc., for helpful discussion and for supplying the samples used in this work.

References and Notes

(1) Nozik, A. J. *Annu. Rev. Phys. Chem.* **1978**, *29*, 189.
(2) Heller, A. *Acc. Chem. Res.* **1981**, *14*, 154.
(3) Rajeshwar, K.; Singh, P.; DuBow, J. *Electrochim. Acta* **1978**, *23*, 1117.
(4) Tomkiewicz, M.; Fay, H. *Appl. Phys.* **1979**, *18*, 1.
(5) Wrighton, M. S. *Acc. Chem. Res.* **1979**, *12*, 303.
(6) Bard, A. J. *Science* **1980**, *207*, 139.
(7) Parkinson, B. *Acc. Chem. Res.* **1984**, *17*, 431.
(8) Gerischer, H. In *Photoelectrochemistry, Photocatalysis and Photoreactors: Fundamentals and Developments*; Schiavello, M., Ed.; D. Reidel: Dordrecht, 1985; Vol. 146, p 39.
(9) Hamnett, A. In *Comprehensive Chemical Kinetics*; Compton, R. G., Ed.; Elsevier: New York, 1987; Vol. 27, p 61.
(10) Finklea, H. O. *Semiconductor Electrodes*; Elsevier: New York, 1988.
(11) Memming, R. In *Electrochemistry II*; Steckhan, E., Ed.; Springer-Verlag: New York, 1988; Vol. 143; p 79.
(12) Pleskov, Y. V. *Solar Energy Conversion*; Springer-Verlag: Berlin, 1990; p 163.
(13) Tan, M. X.; Laibinis, P. E.; Nguyen, S. T.; Kesselman, J. M.; Stanton, C. E.; Lewis, N. S. *Prog. Inorg. Chem.* **1994**, *41*, 21.
(14) Closs, G. L.; Calcaterra, L. T.; Green, N. J.; Penfield, K. W.; Miller, J. R. *J. Phys. Chem.* **1986**, *90*, 3673.
(15) Leland, B. A.; Joran, A. D.; Felker, P. M.; Hopfield, J. J.; Zewail, A. H.; Dervan, P. B. *J. Phys. Chem.* **1985**, *89*, 5571.
(16) Mayo, S. L.; Ellis, W. R.; Crutchley, R. J.; Gray, H. B. *Science* **1986**, *233*, 948.
(17) Willig, F.; Charlé, K.-P. *Mol. Cryst. Liq. Cryst.* **1986**, *137*, 329.
(18) Oevering, H.; Paddon-Row, M. N.; Heppener, M.; Oliver, A. M.; Cotsaris, E.; Verhoeven, J. W.; Hush, N. S. *J. Am. Chem. Soc.* **1987**, *109*, 3258.
(19) Finckh, P.; Heitele, H.; Volk, M.; Michel-Beyerle, M. E. *J. Phys. Chem.* **1988**, *92*, 6584.
(20) *Photoinduced Electron Transfer*; Fox, M. A., Chanon, M., Eds.; Elsevier: Amsterdam, 1988; Vol. Pt. D.
(21) Axup, A. W.; Albin, M.; Mayo, S. L.; Crutchley, R. J.; Gray, H. B. *J. Am. Chem. Soc.* **1988**, *110*, 435.
(22) Isied, S. S.; Vassilian, A.; Wishart, J. F.; Creutz, C.; Schwarz, H. A.; Sutin, N. *J. Am. Chem. Soc.* **1988**, *110*, 635.
(23) Gust, D.; Moore, T. A. *Science* **1989**, *244*, 35.
(24) Wasielewski, M. R. *Chem. Rev.* **1992**, *92*, 435.
(25) Gregg, B. A.; Kim, Y. I. *J. Phys. Chem.* **1994**, *98*, 2412.
(26) Keller, S. W.; Johnson, S. A.; Brigham, E. S.; Yonemoto, E. H.; Mallouk, T. E. *J. Am. Chem. Soc.* **1995**, *117*, 12879.
(27) De la Rosa, M. A.; Navarro, J. A.; Roncel, M. *Appl. Biochem. Biotechnol.* **1991**, *30*, 61.
(28) Vermeulen, L. A.; Thompson, M. E. *Nature* **1992**, *358*, 656.
(29) Borja, M.; Dutta, P. K. *Nature* **1993**, *362*, 43.
(30) Grätzel, M. *MRS Bull.* **1993**, *18*, 61.
(31) Bard, A. J.; Fox, M. A. *Acc. Chem. Res.* **1995**, *28*, 141.
(32) Königstein, C. *J. Photochem. Photobiol. A: Chem.* **1995**, *90*, 141.
(33) Goc, J.; Hara, M.; Tateishi, T.; Miyake, J. *J. Photochem. Photobiol. A: Chem.* **1996**, *93*, 137.
(34) Byrd, H.; Suponeva, E. P.; Bocarsly, A. B.; Thompson, M. E. *Nature* **1996**, *380*, 610.
(35) Gerischer, H. *Adv. Electrochem. Electrochem. Eng.* **1961**, *1*, 139.
(36) Lewis, N. S. *Am. Sci.* **1995**, *83*, 534.
(37) Gärtner, W. W. *Phys. Rev.* **1959**, *116*, 84.
(38) Reichman, J. *Appl. Phys. Lett.* **1980**, *36*, 574.
(39) Ellis, A. B. In *Chemistry and Structure at Interfaces: New Laser and Optical Techniques*; Hall, R. B.; Ellis, A. B., Eds.; VCH: Deerfield Beach, FL, 1986; p 245.
(40) Smandek, B.; Chmiel, G.; Gerischer, H. *Ber. Bunsen-Ges. Phys. Chem.* **1989**, *93*, 1094.
(41) Chmiel, G.; Gerischer, H. *J. Phys. Chem.* **1990**, *94*, 1612.
(42) Licht, S.; Peramunage, D. *Nature* **1990**, *345*, 330.
(43) Seshadri, G.; Chun, J. K. M.; Bocarsly, A. B. *Nature* **1991**, *352*, 508.
(44) Gibbons, J. F.; Cogan, G. W.; Gronet, C. M.; Lewis, N. S. *Appl. Phys. Lett.* **1984**, *45*, 1095.
(45) Rosenbluth, M. L.; Lieber, C. M.; Lewis, N. S. *Appl. Phys. Lett.* **1984**, *45*, 423.
(46) Sze, S. M. *The Physics of Semiconductor Devices;* 2nd ed.; John Wiley and Sons: New York, 1981.
(47) Fonash, S. J. *Solar Cell Device Physics*; Academic: New York, 1981.
(48) Fahrenbruch, A. L.; Bube, R. H. *Fundamentals of Solar Cells: Photovoltaic Solar Energy Conversion*; Academic: New York, 1983.
(49) Rosenbluth, M. L.; Lewis, N. S. *J. Am. Chem. Soc.* **1986**, *108*, 4689.
(50) Dziewior, J.; Schmid, W. *Appl. Phys. Lett.* **1977**, *31*, 346.
(51) Dziewior, J.; Silber, D. *Appl. Phys. Lett.* **1979**, *35*, 170.
(52) Yablonovitch, E.; Gmitter, T. *Appl. Phys. Lett.* **1986**, *49*, 587.

(53) Bard, A. J. *J. Photochem.* **1979**, *10*, 59.
(54) Sakata, T.; Kawai, T. *Nouv. J. Chim.* **1980**, *5*, 279.
(55) Amouyal, M. In *Homogeneous and Heterogeneous Photocatalysis*; Pelizzetti, E., Serpone, N., Eds.; D. Reidel: Dordrecht, 1986; Vol. 174, p 253.
(56) Henglein, A. *Chem. Rev.* **1989**, *89*, 1861.
(57) Kamat, P. V. *Chem. Rev.* **1993**, *93*, 267.
(58) Sczechowski, J. G.; Koval, C. A.; Noble, R. D. *J. Photochem. Photobiol. A: Chem.* **1993**, *74*, 273.
(59) Hagfeldt, A.; Grätzel, M. *Chem. Rev.* **1995**, *95*, 49.
(60) Grätzel, M. In *Photocatalysis and Environment: Trends and Applications*; Schiavello, M., Ed.; Kluwer Academic Publishers: Dordrecht, 1988; Vol. 237; p 367.
(61) Henglein, A. *Top. Curr. Chem.* **1988**, *143*, 113.
(62) Fox, M. A. *Acc. Chem. Res.* **1983**, *16*, 314.
(63) Henglein, A. *Pure Appl. Chem.* **1984**, *56*, 1215.
(64) Pichat, P. In *Photocatalysis and Environment: Trends and Applications*; Schiavello, M., Ed.; Kluwer Academic Publishers: Dordrecht, 1988; Vol. 237, p 399.
(65) Pelizzetti, E.; Pramauro, E.; Minero, C.; Serpone, N.; Borgarello, E. In *Photocatalysis and Environment: Trends and Applications*; Schiavello, M., Ed.; Kluwer Academic Publishers: Dordrecht, 1988; Vol. 237, p 469.
(66) Fox, M. A. *CHEMTECH* **1992**, 680.
(67) Ollis, D. F. In *Emerging Technologies in Hazardous Waste Management III*; Tedder, D. W., Pohland, F. G., Eds.; American Chemical Society: Washington, DC, 1993; Vol. 518.
(68) Hoffmann, M. R.; Martin, S. T.; Choi, W.; Bahnemann, D. W. *Chem. Rev.* **1995**, *95*, 69.
(69) Heller, A. *Acc. Chem. Res.* **1995**, *28*, 503.
(70) Jacoby, W. A.; Blake, D. M.; Noble, R. D.; Koval, C. A. *J. Catal.* **1995**, *157*, 87.
(71) Vinodgopal, K.; Kamat, P. V. *CHEMTECH* **1996**, *26*, 18.
(72) Yamashita, H.; Ichihashi, Y.; Harada, M.; Stewart, G.; Fox, M. A.; Anpo, M. *J. Catal.* **1996**, *158*, 97.
(73) Serpone, N.; Borgarello, E.; Grätzel, M. *J. Chem. Soc., Chem. Commun.* **1984**, 342.
(74) Sakata, T. In *Photocatalysis—Fundamentals and Applications*; Serpone, N., Pelizzetti, E., Eds.; Wiley: New York, 1989; p 311.
(75) Tan, M. X.; Kenyon, C. N.; Lewis, N. S. *J. Phys. Chem.* **1994**, *98*, 4959.
(76) Tan, M. X.; Kenyon, C. N.; Wilisch, W. C. A.; Lewis, N. S. *J. Electrochem. Soc.* **1995**, *142*, L62.
(77) Shockley, W. *Electrons and Holes in Semiconductors*; Van Nostrand: New York, 1950.
(78) Gerischer, H. In *Physical Chemistry: An Advanced Treatise*; Eyring, H. , Henderson, D., Yost, W., Eds.; Academic: New York, 1970; Vol. 9A, p 463.
(79) Memming, R. In *Electron Transfer I*; Mattay, J., Ed.; Springer-Verlag: Berlin, 1994; Vol. 169, p 105.
(80) Gregg, B. A.; Fox, M. A.; Bard, A. J. *J. Phys. Chem.* **1990**, *94*, 1586.
(81) Liu, C. Y.; Pan, H. I.; Fox, M. A.; Bard, A. J. *Science* **1993**, *261*, 897.
(82) Liu, C. Y.; Pan, H. L.; Tang, H.; Fox, M. A.; Bard, A. J. *J. Phys. Chem.* **1995**, *99*, 7632.
(83) Calabrese, G. S.; Lin, M.-S.; Dresner, J.; Wrighton, M. S. *J. Am. Chem. Soc.* **1982**, *104*, 2412.
(84) Harrison, D. J.; Calabrese, G. S.; Ricco, A. J.; Dresner, J.; Wrighton, M. S. *J. Am. Chem. Soc.* **1983**, *105*, 4212.
(85) Hodes, G.; Howell, I. D. J.; Peter, L. M. *J. Electrochem. Soc.* **1992**, *139*, 3136.
(86) Södergren, S.; Hagfeldt, A.; Olsson, J.; Lindquist, S. E. *J. Phys. Chem.* **1994**, *98*, 5552.
(87) Grätzel, M. *Proc. Indian Acad. Sci. (Chem. Sci.)* **1995**, *107*, 607.
(88) Matson, R. J.; Emery, K. A.; Bird, R. E. *Sol. Cells* **1984**, *11*, 105.
(89) Lewis, N. S. *J. Electrochem. Soc.* **1984**, *131*, 2496.
(90) Dash, W. C.; Newman, R. *Phys. Rev.* **1955**, *99*, 1151.
(91) Hovel, H. J. *Solar Cells*; Academic Press: New York, 1975; Vol. 11, p 254.
(92) Weakliem, H. A.; Redfield, D. *J. Appl. Phys.* **1979**, *50*, 1491.
(93) Saritas, M.; McKell, H. D. *J. Appl. Phys.* **1987**, *61*, 4923.
(94) *Optical Functions of Intrinsic Si*; Aspnes, D. E., Ed.; INSPEC: London, 1988.
(95) Bücher, K.; Bruns, J.; Wagemann, H. G. *J. Appl. Phys.* **1994**, *75*, 1127.
(96) Kumar, A.; Lewis, N. S. *J. Phys. Chem.* **1990**, *94*, 6002.
(97) Fajardo, A. M.; Karp, C. D.; Kenyon, C. N.; Pomykal, K. E.; Shreve, G. A.; Tan, M. X.; Lewis, N. S. *Sol. Energy Mater. Sol. Cells* **1995**, *38*, 279.
(98) Forbes, M. D. E.; Lewis, N. S. *J. Am. Chem. Soc.* **1990**, *112*, 3682.
(99) Kumar, A.; Lewis, N. S. *Appl. Phys. Lett.* **1990**, *57*, 2730.
(100) Morrison, S. R. *Electrochemistry at Semiconductor and Oxidized Metal Electrodes*; Plenum Press: New York, 1980.
(101) Shreve, G. A.; Lewis, N. S. *J. Electrochem. Soc.* **1995**, *142*, 112.
(102) Gerischer, H. In *Solar Energy Conversion. Solid-State Physics Aspects*; Seraphin, B. O., Ed.; Springer-Verlag: Berlin, 1979; Vol. 31, p 115.

(103) Even if $\Delta n \geq p_{so}$, V_{n+} is very large, but V_{p+} deviates from zero because holes must build up relative to their equilibrium values in order to achieve an open-circuit condition.

(104) In principle, it should be possible to obtain separate values for the exchange current densities simply by measuring simultaneously the net current and the voltages at the n^+ and p^+ points. Unfortunately, this is complicated because *IR* losses in the electrolyte affect the measured voltages, especially at higher currents.